Photostability Via Sloped Conical Intersections: A Computational Study of the Excited States of the Naphthalene Radical Cation

Katherine F. Hall, Martial Boggio-Pasqua, Michael J. Bearpark,* and Michael A. Robb

Contribution from Imperial College London, Chemistry Department, South Kensington Campus, London SW7 2AZ, U.K.

Received: July 24, 2006; In Final Form: October 9, 2006

On the basis of an extensive ab initio electronic structure study of the ground and excited-state potential energy surfaces of the naphthalene radical cation ($N^{\bullet+}$), we propose a mechanism for its ultrafast nonradiative relaxation from the second excited state (D_2) down to the ground state (D_0), which could explain the experimentally observed photostability [Zhao, L.; Lian, R.; Shkrob I. A.; Crowell, R. A.; Pommeret, S.; Chronister, E. L.; Liu, A. D.; Trifunac, A. D. *J. Phys. Chem. A.*, 2004, *108*, 25]. The proposed photophysical relaxation pathway involves internal conversion from the D_2 state down to the D_0 state via two consecutive, accessible, sloped conical intersections (CIs). The two crossings, D_0/D_1 and D_1/D_2, are characterized at the complete active space self-consistent field (CASSCF) level. At this level of theory, the D_0/D_1 crossing is energetically readily accessible, while the D_1/D_2 CI appears too high in energy to be involved in internal conversion. However, the inclusion of dynamic correlation effects, via single point CASPT2 calculations including excitations out of the valence π- and σ-orbitals, lowers the D_0 and D_2 state energies with respect to D_1. Extrapolations at the CASPT2 level predict that the D_1/D_2 crossing is then significantly lower in energy than with CASSCF indicating that with a higher-level treatment of dynamic correlation it may be energetically accessible following vertical excitation to D_2. $N^{\bullet+}$ is proposed as one of the species contributing to a series of diffuse infrared absorption bands originating from interstellar clouds. Understanding the mechanism for photostability in the gas phase, therefore, has important consequences for astrophysics.

Introduction

The main aim of this study is to present a consistent mechanism for the photophysics of the naphthalene radical cation, a highly photostable, nonfluorescing, cationic polycyclic aromatic hydrocarbon (PAH). Very little is known about the photophysics and reactivity of PAH radical cations, partly because of their inherent nonfluorescence and difficulties in isolating the charged species. Gas-phase photofragmentation studies of a variety of PAH monocations have shown the high photostability of these species (dissociation onsets of 4−4.5 eV) and suggest fast relaxation times.[1]

PAHs and their cations have been extensively studied because of their wide-ranging scientific interest. Recent research concerns their possible role as intermediates in a range of reactions including the formation of molecular hydrogen,[2] the growth of large carbon structures such as fullerenes,[3] and their use in molecular electronic devices including molecular wires[4] and the pentacene transistor.[5]

Currently, the most prevalent experimental and theoretical studies of PAH cations concern their possible existence in the interstellar medium (ISM) in which they are proposed as candidates for a number of infrared (IR) absorption and emission bands. In the literature, some confusion arises about the distinction between vibrational IR spectra and electronic IR spectra, which can often overlap in energy due to the small D_0-D_1 gap in these species. While small PAH cations are electronically nonfluorescent, displaying fast internal conversion to the ground state, the radiative vibrational relaxation spectra of a number of PAH cations have been studied using matrix-isolated absorption spectroscopy and gas-phase radiative cooling kinetics.[6] These emission spectra are linked to the interstellar unidentified infrared (UIR) bands. Our interest, however, is in the electronic excitations of PAH cations, which have been linked to a number of absorption features, superposed on the spectra of early type reddened OB stars, known as the diffuse interstellar bands (DIBs). Discovered in 1922 by Heger,[7] there are some 300 DIBs originating from interstellar clouds and ranging from the near ultra-violet (UV) to the near IR (4400−10 000 Å). Their characterization is one of the most enduring problems in astrophysical spectroscopy.

There is a current consensus that DIBs are caused by organic molecules and their ions present in interstellar clouds. PAH cations are particularly promising candidates owing to their inherent photostability and believed abundance in the ISM in which a large fraction of the molecules are expected to be ionized by the high flux of UV radiation. The $\pi \rightarrow \pi$ absorptions of a range of PAH cations, identified both in experimental and theoretical spectroscopic studies, fall within the astronomical frequency range of interest, and several matches have been made between observed DIBs and PAH cation absorption frequencies but no conclusive assignments have been made. (For reviews, see ref 8.)

Difficulty in isolating the cations in the gas phase has meant that the majority of spectroscopic work has been performed in low temperature inert gas matrices.[9] The frequency shift associated with the solid framework causes difficulty in assignment to the astronomical data. However, gas-phase experiments have been performed on $N^{\bullet+}$ by Romanini and Biennier et al.

* Corresponding author. E-mail: m.bearpark@imperial.ac.uk.

10.1021/jp064711g CCC: $33.50
Published on Web 11/23/2006

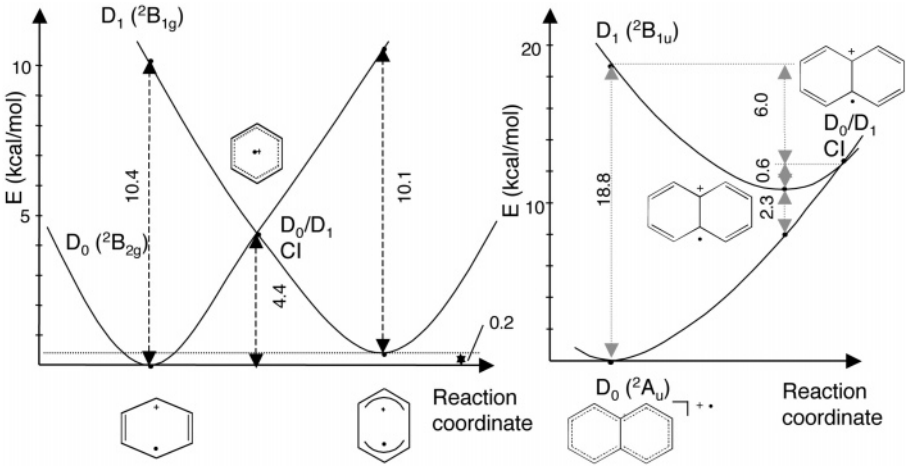

Figure 1. A comparison of the schematic forms of the D_0/D_1 conical intersections of the benzene and naphthalene cations. Calculations performed with CASSCF/6-31G* using Gaussian. Energies in kcal/mol.

and possible matches have been suggested between the $D_0 \rightarrow D_2$ absorption peaks at 6706.5 and 6488.4 Å and the weak DIBs features at 6699.4 and 6491.9 Å, respectively.[10]

There have been several theoretical studies into small PAH cations that have identified with vibrational detail the positions of IR absorption peaks to a high level of accuracy with results comparing well with experiment.[11] Recent ab initio studies of the naphthalene cation include a complete active space self-consistent field (CASSCF) study by Andruniow et al.[11b]. In their study, the ground and two lowest lying excited states ($^2B_{1u}$ and $^2B_{3g}$) were optimized and the vertical excitation energies calculated. Bally et al.[11c] carried out a density functional theory optimization on the ground state of $N^{\bullet+}$ with CASSCF and CASPT2 vertical excitation energies. Their results compared well with electron absorption and photoelectron experiments carried out by the group. A D_0/D_1 energy level crossing was suggested but not characterized in a similar study by Da Silva et al.[11d]

Finding evidence for the involvement of PAH cations in DIBs hinges not only on analysis and calculation of IR spectra, but also on identifying the relevant relaxation mechanisms responsible for the photostability of these cations following absorption. In a recent paper, Zhao et al.[12] studied the relaxation dynamics of cold (10−100 K) $N^{\bullet+}$ isolated in boric acid glass using transient grating (TG) spectroscopy. After absorption of a 680 nm photon to vertically excite to the D_2 state, rapid, efficient relaxation of the photoexcited cation down to its ground state was observed. The TG spectrum was fitted to a biexponential function, revealing two-step relaxation kinetics involving a fast component (<200 fs) and a slow component (3−20 ps). The two steps were interpreted as an initial rapid D_2 to D_0 internal conversion, followed by slow vibrational relaxation of the hot D_0 state. The group further postulated that the observed fast step is due to the $D_1 \rightarrow D_0$ relaxation, concluding that the $D_2 \rightarrow D_1$ relaxation occurs on a time-scale too short to be measured by their apparatus (<1 fs). Although these experiments were performed in matrix-isolated conditions, evidence that the situation is not appreciably different in the gas phase is provided by recent cavity ringdown spectroscopy (CRDS) performed on $N^{\bullet+}$, in which broadening of the absorption peaks was concluded to be consistent with a nonradiative decay process with a lower-limit relaxation time of 212 fs[10a].

To our knowledge, there has been no prior theoretical work explicitly on the photorelaxation mechanism or dynamics of $N^{\bullet+}$, and no work has been attempted to characterize any interstate crossings for this system. It is now an accepted idea that nonavoided crossings (conical intersections) can function as "funnels" between two electronic states allowing ultrafast, radiationless transitions between them. (For a general introduction to potential energy surfaces and crossings, see ref 13). The topology of the crossing has important implications for excited-state lifetime and product formation (see ref 14 for relevant discussion). In particular, sloped CIs (in which we employ the classification system of Ruedenberg et al.[15]) have been associated with photostability. At a sloped intersection, there is a single well-defined energy-lowering coordinate on the lower surface, leading to products. For example, we recently described a mechanism for the photostability of pyracylene via an accessible sloped S_0/S_1 conical intersection leading to reformation of starting material.[16] Azulene also has been demonstrated to decay nonradiatively via a sloped S_0/S_1 crossing, partly explaining the observed fluorescence from the second excited state (S_2) minimum rather than the first (S_1), following vertical excitation.[17]

Much theoretical attention has been given to the D_0/D_1 conical intersection of the benzene radical cation ($B^{\bullet+}$). Its high symmetry (D_{6h}) and small size lend themselves to the study of $B^{\bullet+}$ as a model Jahn−Teller system.[18] The removal of an electron from the degenerate highest occupied molecular orbital (HOMO) of the benzene molecule causes a Jahn−Teller splitting, reducing the symmetry and stabilizing the radical cation. This produces a symmetry-required crossing of the two energy states at a high-symmetry D_{6h} geometry close to that of neutral benzene (Figure 1). The result is a peaked conical intersection. In the moat surrounding the CI, there are two types of symmetry-lowered (D_{2h}) stationary point geometries corresponding to occupation of one or the other of the previously degenerate HOMO π-orbitals.

Naphthalene belongs to the lower symmetry D_{2h} point group, which has no degenerate representations; based on symmetry, we cannot expect a similar behavior to benzene following ionization. However, the radiationless femtosecond relaxation dynamics presented by Zhao et al.[12] strongly indicate the presence of a low-energy crossing between the potential energy surfaces (PESs) of $N^{\bullet+}$. In the relaxation experiments, $N^{\bullet+}$ was isolated in a geometry-restricted solid matrix, which suggests that the geometry changes associated with motion from the Franck−Condon (FC) geometry through any crossings are small, planar bond-length relaxations. The expectation of a lowered D_0-D_1 energy gap for radical cations[19] would also support the possibility of a low-energy crossing. In contrast to the benzene case, we find that the D_0/D_1 CI for $N^{\bullet+}$ is sloped (Figure 1).

Consequently, there is only one relaxation pathway from the crossing down to the ground state minimum, providing part of a mechanism for photostability.

Our investigation consists of the determination of critical points on the ground and first two electronic excited-state potential energy surfaces of $N^{\bullet+}$. After a discussion of computational methods, we will present in detail the results of our CASSCF study with comparison to the experimental observations. This will lead to a discussion of the need to include dynamic correlation effects in the calculations for this system, using post-CASSCF methods. A rationalization of the experimentally observed photostability of the naphthalene cation is then presented.

Computational Details

The ground (D_0) and first three excited states (D_1, D_2, and D_3) of the naphthalene radical cation have been computed using CASSCF by distributing 9 π electrons in the 10 valence π orbitals (9e, 10o).

The π-electronic states belong to the A_u, B_{1u}, B_{3g}, and B_{2g} irreducible representations of the D_{2h} point group, respectively. CASSCF calculations were performed using both Gaussian[20] (without symmetry restrictions) and MOLPRO[21] with symmetry restrictions. The symmetry-restricted calculations on the D_1 minimum and the D_0/D_1 and D_1/D_2 CIs, described below, were carried out with MOLPRO, as were multireference configuration interaction (π-MRCI) and complete active space second-order perturbation (CASPT2) calculations. Where symmetry-restricted calculations were carried out, these are the results quoted below for energy, geometry and gradient vectors.

The basis set used for the CASSCF geometry optimizations was 6-31G*,[22] which includes polarization d-functions on the carbon atoms, as this has been shown to give accurate results in similar studies[16, 18b] and is flexible enough to give a good qualitative description of the covalent excited states of organic molecules. CASSCF energies were re-computed with cc-pVTZ[23] and aug-cc-pVTZ[24] basis sets without re-optimizing geometries.

CASSCF/6-31G* geometry optimizations were performed using CASSCF/STO-3G[25] optimized starting geometries. To optimize the D_1 minimum, state-averaged orbitals with equal weighting between the D_0 and D_1 states were used to prevent root flipping. The D_1 minimum was re-optimized without state-averaging by constraining both the point group symmetry of the molecule to D_{2h} and the irreducible representation of the state to B_{1u}. The optimized minima structures on the D_0 and D_2 states were confirmed to be true energy minima and not saddle points using numerical frequency calculations. This was not feasible for the D_1 state because we were only able to optimize the minimum by constraining the symmetry of the state, and numerical frequency calculations would break the molecular point group symmetry. Numerical frequency calculations using state-averaged orbitals are possible. However, such a computation would require solving the coupled-perturbed multiconfigurational self-consistent field (MCSCF) equations for each single-energy point calculation. Attempts to carry out a numerical frequency calculation without any symmetry or coupled-perturbed corrections failed with orbital convergence problems. We chose not to pursue this further, as the minimum and conical intersection on D_1 are almost co-incident.

We performed single point π-MRCI[26] and CASPT2[27] calculations to explore dynamic correlation effects on the energies of the CASSCF-optimized states. Calculations were performed using a CASSCF reference wave function with single and double excitations out of the valence π-orbitals in the case of MRCI (π-MRCI) and single and double excitations out of the full valence space in the case of the cheaper perturbation method. Comparison between the two multireference methods allowed analysis of the contribution from excitations between the σ- and π-orbitals ($\sigma-\pi$ polarization).

Large basis sets with polarization functions are known to be important in recovering dynamic correlation energy. The π-MRCI and CASPT2 calculations were performed using a 6-31G* basis, as well as the correlation consistent cc-pVTZ and aug-cc-pVTZ basis sets, to analyze basis set convergence.

Conical intersection optimizations[28] require state-averaged orbitals. The orbital rotation derivative correction for such orbitals becomes prohibitively expensive with large active spaces and no symmetry but is expected to be small in most cases and was consequently neglected in the initial CASSCF-crossing optimizations performed in this study. However, by constraining the point group symmetry to D_{2h} and thereby reducing the number of configurations by an order of magnitude, we were able to re-optimize the two crossings using CASSCF including the correction term. A lower energy point on the D_1/D_2 crossing was characterized when the correction term was included. This anomaly was probably due to the near-parallel gradients of the two states in the proximity of the D_1/D_2 crossing, which is characteristic of sloped crossings. However, the D_0/D_1 crossing geometry was unaffected by the correction term.

Transition dipole moment (TDM) calculations were performed with Gaussian using state-averaged orbitals between the three states of interest.

Results and Discussion

The results of our CASSCF calculations are summarized in Figures 2 and 3 and in Table 1.

Figures 2 and 3 show the CASSCF potential energy profiles of the three electronic states involved in the photophysics of the naphthalene cation. These are the ground, D_0 (A_u), and the first two excited states, D_1 (B_{1u}) and D_2 (B_{3g}) (where the label D_n refers to the order obtained for vertical transitions). The potential surface is displayed on two separate diagrams for clarity, because the reaction coordinate is not the same in both cases. The third excited state also was calculated, but is energetically well separated from the other states over the range of interest (Table 1).

All the optimized minima and crossings have D_{2h} point group symmetry, and the structures are drawn up on Figures 2 and 3 and summarized in Table 2. The energy gradient vectors of the states at the FC points and crossings are opposite to the forces acting on the molecule. These are shown in Figures 2 and 3 (right side) to illustrate the driving force for the photophysics and the nature of the reaction coordinate, which is along the symmetry-preserving gradient difference (UGD) vector in each case (Figure 4). (It should be noted that vertical transition to the D_1 state is forbidden by symmetry, and that this value is shown in Figure 2 as a point of reference only.)

The results are structured as follows: first, we will discuss the results of the CASSCF study, describing the first three doublet energy states, D_0, D_1, and D_2, and their optimized equilibrium geometries. We then describe the form of the PES with reference to the energies of the critical points at the CASSCF level and the effect of the inclusion of dynamic correlation (CASPT2 energies summarized in Table 3). The electronic nature of both the ground and second excited states means that including dynamic correlation is necessary to obtain excitation energies that agree closely with experiment. The results are collected into a mechanism for the experimentally observed photophysics of the naphthalene cation.

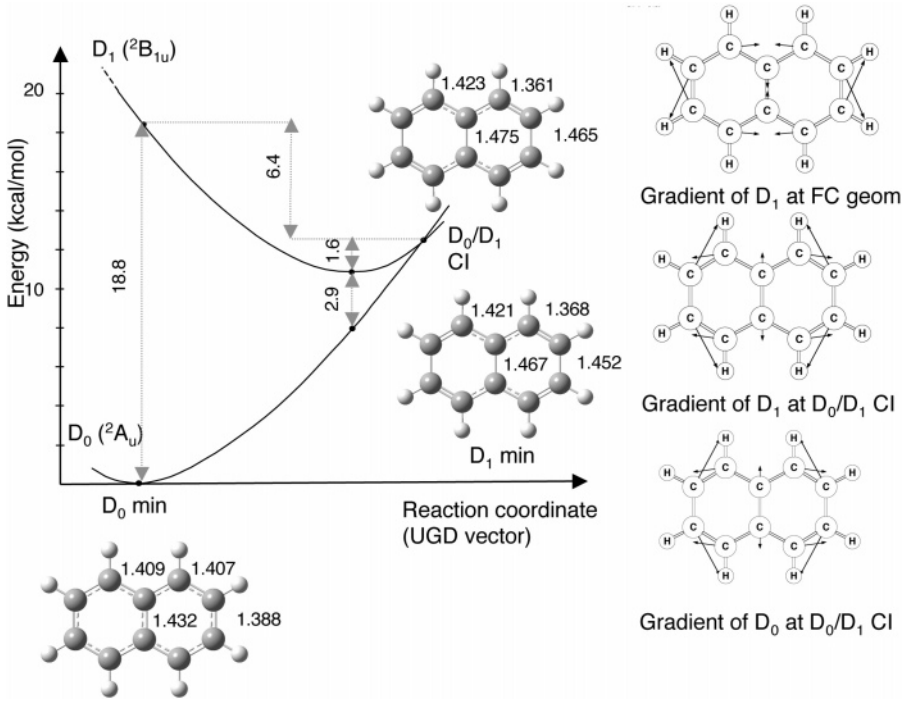

Figure 2. Critical points optimized on the D_0 and D_1 states of the naphthalene radical cation using CASSCF/6-31G*. Energies in kcal/mol. Vectors to the right display the energy gradients at the intersection and FC geometry.

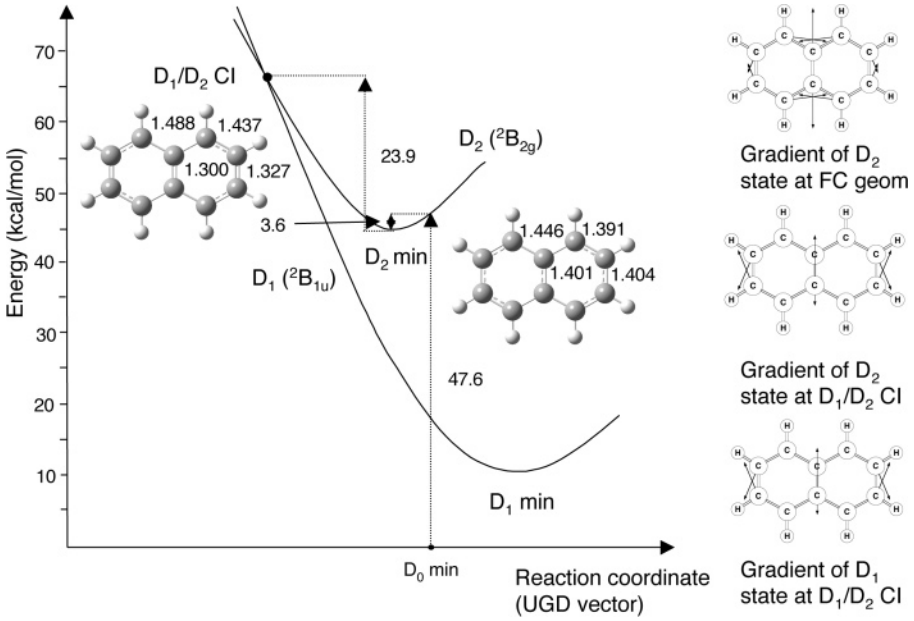

Figure 3. Critical points optimized on the D_1 and D_2 states of the naphthalene radical cation using CASSCF/6-31G*. Energies in kcal/mol. Vectors to the right display the energy gradients at the intersection and FC geometry.

Analysis of the major configurations contributing to the excited-state wave functions reveals that the three lowest lying states (D_0 to D_2) correspond primarily to the single occupation of the π_5, π_4, and π_3 bonding orbitals, respectively (Figure 5). While all the equilibrium structures are planar and belong to the D_{2h} point group, each state has a distinctive pattern of carbon−carbon bond length alternation. These bond length differences are reflected in the shape of the singly-occupied delocalized π-MO (SOMO) in each state.

The bond lengths in italics in Table 2 are shown for comparison and are taken from the experimentally determined geometry[29] in the case of the neutral species and from the full optimized reaction space (FORS)−MCSCF calculations of Andruniow et al.[11b] for the cation structures. The two sets of results for the cation are in good agreement with our results showing an average systematic shortening of about 0.008 Å compared with

TABLE 1: Energies of States D_1 to D_3 of Optimized Critical Points of the Naphthalene Radical Cation Calculated Using CASSCF(9,10)/6-31G* Relative to the D_0 State at the Optimized D_0 Minimum Geometry[a]

geometry	D_0	D_1	D_2	D_3	T_e
D_0 minimum	0.0	18.8	47.6	67.2	0.0
D_1 minimum	8.0	10.8	51.3	69.0	10.8
D_2 minimum	3.5	18.1	44.0	70.2	44.0
D_3 minimum	2.4	15.0	48.8	65.6	65.6
D_0/D_1 CI	12.4	12.4	54.0	70.8	
D_1/D_2 CI	31.1	68.0	68.0	88.4	

[a] Energies in kcal/mol. T_e are the adiabatic excitation energies.

TABLE 2: Carbon−Carbon Bond Lengths for the Optimized Critical Points on the PESs of the Naphthalene Radical Cation Calculated Using CASSCF/6-31G*[a]

	Critical point										
bond	neutral		D_0 min		D_1 min		D_2 min		D_3 min	D_0/D_1 CI	D_1/D_2 CI
R_1	1.416	*1.417*	1.432	*1.438*	1.467	*1.475*	1.401	*1.407*	1.447	1.471	1.300
R_2	1.427	*1.425*	1.409	*1.416*	1.421	*1.429*	1.446	*1.455*	1.413	1.423	1.488
R_3	1.373	*1.377*	1.407	*1.417*	1.368	*1.379*	1.391	*1.402*	1.408	1.363	1.437
R_4	1.421	*1.417*	1.388	*1.398*	1.452	*1.461*	1.404	*1.415*	1.434	1.470	1.327

[a] Bond lengths in angstroms. Labels refer to Chart 1. All critical points are of D_{2h} symmetry. Bond lengths in italics are taken from the experimentally determined geometry of Brock et al.[29] in the case of the neutral species and from the FORS−MCSCF calculations of Andruniow et al.[11b] for the cation structures.

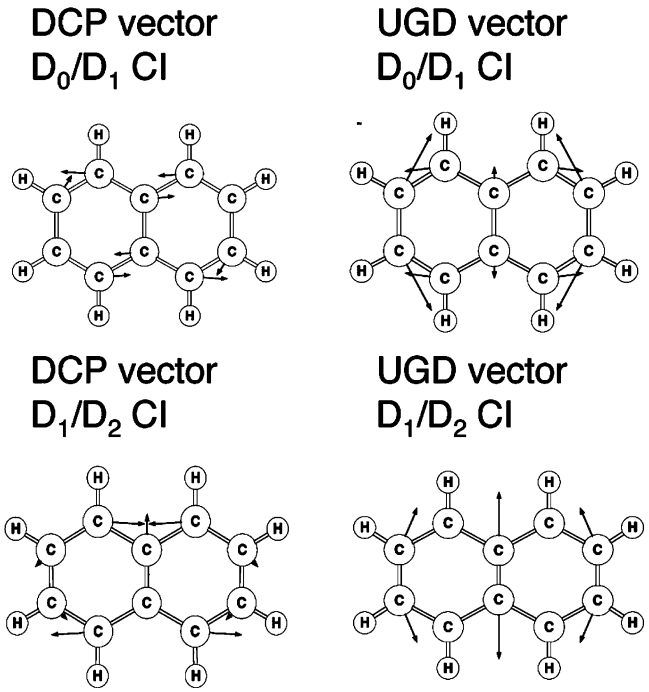

Figure 4. The branching space coordinates (UGD and DCP) of the D_0/D_1 and the D_1/D_2 conical intersections of the naphthalene cation.

the Andruniow results, which is consistent with the larger basis set used in our calculations (6-31G* compared with DZV). (Our calculated excitation energies also agree within 1 kcal/mol).

Examining the bond lengths in Table 2, we see that ionization of the neutral naphthalene to the cation is accompanied by small, planar bond length relaxations, and the D_{2h} symmetry is retained. Because the ground electronic state of naphthalene is not degenerate, we do not necessarily expect to see symmetry breaking upon ionization as is the case with Jahn−Teller systems like benzene[18b].

Ionization occurs from the π_5 orbital of the neutral molecule (Figure 5) to give the ground state of the cation. When an electron is removed from the π_5 orbital, the localization of electron density around the R_3 bonds is decreased while the antibonding character in the R_4 bonds is decreased (Chart 1). Consequently, the R_3 bonds are longer and the R_4 bonds shorter than in the neutral species.

The first excited state of the cation corresponds to excitation of an electron from π_4 into π_5. This is a symmetry forbidden transition. D_1 is therefore a "dark" state with $D_0 \rightarrow D_1$ TDM calculated to be 0.000 au. Vertical transition to the D_1 state would cause the electron density to increase around the R_3 bonds and decrease around the R_1 and R_4 bonds, leading to relaxation to the minimum structure on this state involving compression of the R_3 bonds and elongation of the R_1 and R_4 bond lengths, accompanied by an 8 kcal/mol lowering in the energy of the state (Figure 2).

The allowed photoexcitation to the D_2 state from the ground state (TDM = 0.997 au) corresponds to moving an electron from the π_3 orbital into the π_5 orbital, reducing the electron density around the R_2 bonds and decreasing the antibonding character in the R_1 bond. Relaxation to the D_2 minimum from the FC geometry, therefore, involves elongation of the R_2 bonds and compression of the R_1 bond with a lowering of the D_2 state energy of just 3.6 kcal/mol (Figure 3). The D_2 state has a minimum closer in structure to that of the D_0 minimum than does the D_1 state. This can be rationalized by the observation of the shared *xz*-nodal plane in the SOMOs of the D_0 and D_2 states (π_3 and π_5, respectively).

The small energy gap (2.9 kcal/mol) between the D_0 and D_1 states at the D_1 minimum suggests the existence of a nearby state crossing. A sloped conical intersection was located just 1.6 kcal/mol above the D_1 minimum (0.6 kcal/mol above the state-averaged D_1 min.). This crossing can be rationalized by analysis of the effect on the energies of the two states of the relaxation coordinate from the FC geometry on D_1. Motion along this coordinate from the D_0 minimum causes a sharp increase in the D_0 state energy, while the D_1 energy decreases toward the minimum leading to a crossing between the two states lying along the same coordinate just beyond the D_1 minimum geometry (Figure 2). The force vectors (opposite of the energy gradient vectors illustrated in Figure 2) of the D_1 state at the FC geometry and that of the D_0 and D_1 states at the optimized D_0/D_1 CI all lie along the same symmetry preserving coordinate (UGD vector in Figure 4). This indicates that relaxation through the crossing from the D_1 state to the ground state is along a single well-defined coordinate involving mainly compression of R_3 and extension of R_4 and R_1 (Table 2) and requiring little re-distribution of energy. Our results support an ultrafast relaxation pathway between the D_1 and the D_0 states in full agreement with the observed relaxation step in the experimental results, to which a time period of 200 fs was fitted. The small energy barrier to the crossing on the D_1 state would make fluorescence from this state very difficult to achieve, supporting the lack of fluorescence seen in experiment.

The experimental excitation is to D_2, and so we now turn our attention to the reaction path for relaxation from this state. We optimized a crossing between the D_1 and D_2 states (Figure 3). This crossing also is found to be sloped, again with the two states having almost parallel energy gradients. However, in this instance, the energy of the CI structure is 23.9 kcal/mol above the D_2 minimum and 20.3 kcal/mol higher than the energy of the FC point for this state. The crossing appears, therefore, to be energetically inaccessible following vertical excitation to the D_2 state based on CASSCF calculations. Part of the reason for the high energy of this D_1/D_2 crossing structure is the unusually short R_1 bond (1.30 Å). Analysis of the geometrical coordinates leading from the FC point to the minimum on this state and from the minimum to the crossing show that the reaction path is not along a single coordinate as was the case for the

TABLE 3: Energies of the Critical Points on the D_n States of the Naphthalene Radical Cation Recomputed Using CASSCF(9,10), π-MRCI, and CASPT2 with 6-31G* and cc-pVTZ Basis Sets[a]

	CASSCF(9,10)			π-MRCI		CASPT2	
ΔE (kcal/mol)	6-31G*	sa	cc-pVTZ	6-31G*	cc-pVTZ	6-31G*	cc-pVTZ
$D_0 \rightarrow D_1$ vertical	18.8		18.6	20.7	21.1	23.5	23.4
$D_0 \rightarrow D_1$ adiabatic	10.8	*12.2*	10.6	13.0	13.5	16.7	16.9
$\Delta E(D_1\text{-}D_0)$ at D_1 min	2.9	*2.3*	2.6	5.0	5.5	10.0	10.2
$\Delta E(D_1\text{-}D_0)$ at D_0/D_1 CI	0.0		0.3	2.1	2.6	7.5	7.8
$\Delta E(D_1)$ at D_0 min	8.0	*6.6*	8.0	7.7	7.6	6.8	6.5
$\Delta E(D_1)$ at D_0/D_1 CI	1.6	*0.6*	0.2	0.3	0.3	0.4	0.4
$D_0 \rightarrow D_2$ vertical	47.6		46.8	48.9		47.6	46.9
$D_0 \rightarrow D_2$ adiabatic	44.0		43.5	45.4		43.7	43.4
$\Delta E(D_2\text{-}D_1)$ at D_2 min	25.8		24.7	24.5		20.1	19.4
$\Delta E(D_2\text{-}D_1)$ at D_1/D_2 CI	0.0		0.3	−1.6		−6.0	−6.6
$\Delta E(D_2)$ at D_0 min	3.6		3.3	3.5		3.9	3.5
$\Delta E(D_2)$ at D_1/D_2 CI	23.9		23.0	24.0		22.0	21.4

[a] All critical point geometries optimized using CASSCF(9,10)/6-31G*. ΔE (D_n-D_m) are the energy differences between state D_n and state D_m at the geometry specified. ΔE (D_n) are the relative energies of the state D_n at the geometry specified with respect to the energy at the D_n minimum. Energies in kcal/mol. The energies for the D_1 minimum optimized using state-averaged (sa) orbitals are shown for reference in column 3.

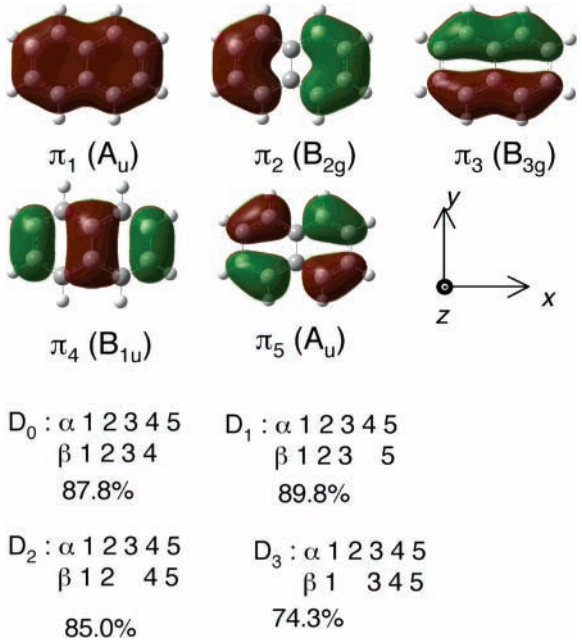

Figure 5. The five valence bonding π-orbitals of the naphthalene cation together with the major configurations contributing to the D_0, D_1, D_2, and D_3 wave functions. The percentage contribution to the wave function at the minimum of each state calculated with CASSCF is given.

CHART 1

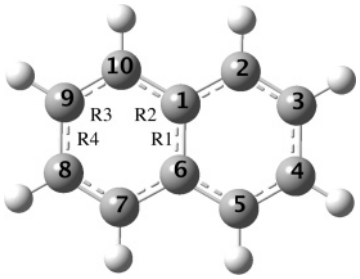

D_0/D_1 CI. The largest change is seen in the remarkable compression of the R_1 bond, which decreases progressively from the FC point to the crossing, while the R_2 bond is seen to increase progressively along the reaction path. However, the changes in the R_3 and R_4 bonds are not consistent along the reaction path (Table 2). This also is shown in the differences in the energy-gradient vectors at the FC point and crossing, shown in Figure 3.

The branching space coordinates for the optimized D_0/D_1 and D_1/D_2 crossings (UGD and derivative coupling (DCP)) are illustrated in Figure 4. These are the two coordinates from $3N$-6 (where N is the number of atoms) that lift the degeneracy between the two states and are orthogonal to the ($3N$-8)-dimensional intersection seam. The reaction coordinates in Figures 2 and 3 correspond primarily to UGD vectors in each case, preserving the symmetry and indicating that the reaction path through each crossing lies in the orthogonal branching space at the minimum on the intersection seam.[15,30]

To check the reliability of the CASSCF energies, higher-level calculations were performed to assess the effect of dynamic correlation on the relative energies of the three states. The reason for doing so is to ensure a balanced description of all three states. CASSCF is capable of describing the qualitative features of covalent excited states. However, for excited states displaying differences in charge separation, the contribution from dynamic correlation energy becomes very important and is not well described by the CASSCF wave function. The higher than expected energy of the D_1/D_2 crossing indicates a need to check that the D_1 and D_2 states are being described in a balanced way.

Two approaches were used to recover the dynamic correlation energy. First, contracted π-MRCI including single and double excitations out of the valence π-orbitals of the reference CASSCF wave function was used. However, this approach cannot recover polarization effects between the valence σ- and π-orbitals. A perturbation theory approach was therefore employed, allowing all single and double excitations out of the full CASSCF wave function (CASPT2). The results are summarized in Table 3.

The CASPT2 calculations significantly reduce the energies of the D_0 and D_2 states relative to the D_1 state, compared with the CASSCF results: the energy differences between D_0 and D_1 at the minima on each state are increased by 5 and 7 kcal/mol, respectively, with CASPT2, while the energy differences between the D_0 and D_2 states are unaffected by the dynamic correlation effects (Table 3). An analysis of the correlation energies at the CASPT2 level revealed that there is a greater correlation effect in the D_0 and D_2 states compared to the D_1 state, explaining this relative difference from the CASSCF results, and perhaps suggesting some extra ionic character in these states. The same effect was not observed in

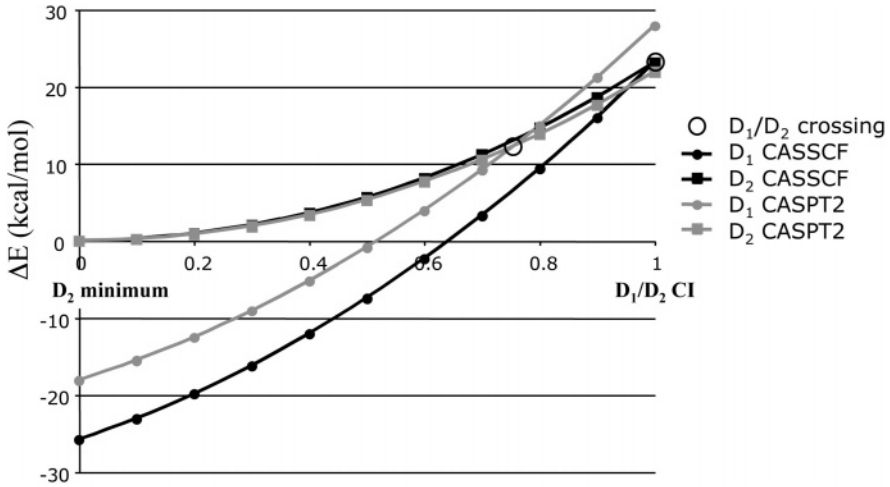

Figure 6. Linear interpolation between the D_2 minimum and D_1/D_2 CI optimized with CASSCF(9,10)/6-31G*, showing the proposed lowering of the energy of the crossing when the $\sigma-\pi$ dynamic correlation effects are included in the calculation using CASPT2/6-31G*.

TABLE 4: Energies of the CASSCF/6-31G* Optimized Critical Points of the Naphthalene Radical Cation Recomputed Using CASSCF and CASPT2 with 6-31G*, cc-pVTZ, and Aug-cc-pVTZ Basis Sets[a]

		$D_2(B_{3g})$ min			$D_1(B_{1u})/D_2(B_{3g})$ CI		
method	basis set	$D_1(B_{1u})$	$D_2(B_{3g})$	$\Delta E(D_2-D_1)$ (kcal/mol)	$D_1(B_{1u})$	$D_2(B_{3g})$	$\Delta E(D_2-D_1)$ (kcal/mol)
CASSCF	6-31G*	−383.18604	−383.14486	25.8	−383.10675	−383.10673	0.0
	cc-pVTZ	−383.29816	−383.25873	24.7	−383.22252	−383.22211	0.3
	aug-cc-pVTZ	−383.29995	−383.26051	24.7	−383.22252	−383.22211	0.3
CASPT2	6-31G*	−384.30384	−384.27183	20.1	−384.22718	−384.23675	−6.0
	cc-pVTZ	−384.71470	−384.68376	19.4	−384.63917	−384.64968	−6.6
	aug-cc-pVTZ	−384.73347	−384.70652	16.9	−384.66235	−384.67304	−6.7

[a] Absolute energies in Hartrees and relative energies in kcal/mol.

the π-MRCI calculations, indicating that the dominating effect is $\sigma-\pi$ polarization. A similar dynamic correlation effect was seen in the ionic S_2 state of pyracylene.[16]

Experimentally, there are several matrix isolated electron absorption spectra (MIS) for $N^{\bullet+}$ that all assign the strongest absorption band to the (0−0) absorption to D_2 (42.4 kcal/mol[9b] in Ne). This is consistent with the small geometry changes calculated on going from D_0 to D_2 minima (Table 2). A gas phase absorption spectrum was obtained using cavity ringdown spectroscopy[10a] and is shifted by only 0.2 kcal/mol from the MIS result. The strongest absorption peak (42.6 kcal/mol) is again assigned to the band origin (0−0), which is within 1 kcal/mol of our CASPT2 adiabatic excitation energy (43.6 kcal/mol). There are no direct experimental results for the symmetry forbidden electronic absorption to D_1. However, our calculated $D_0 \rightarrow D_1$ adiabatic excitation energy (16.9 kcal/mol) is within 1 kcal/mol of the I_2-I_1 photoelectron ionization energy (17.9 kcal/mol[31]).

Because of the near-parallel gradients of the D_1 and D_2 states near the D_1/D_2 CI, the relative shift in the energies of these two states causes the energy gap at the CASSCF/6-31G* optimized crossing geometry to increase to 6 kcal/mol with CASPT2 (Table 3). It is expected, therefore, that the optimized D_1/D_2 crossing geometry would be significantly relaxed if optimized using CASPT2 rather than CASSCF, reducing the energy barrier to the crossing. A linear interpolation to the crossing point using CASPT2/6-31G* suggests that the true D_1/D_2 CI may be more than 10 kcal/mol lower in energy than the CASSCF calculated crossing (Figure 6), as the crossing occurs "earlier" along the interpolation coordinate, and this represents an upper bound to the CASPT2/6-31G* crossing energy.

This analysis is not conclusive, but with the effects of geometry relaxation, it is suggestive that the D_1/D_2 crossing may become accessible and allow for ultrafast nonradiative decay through the conical intersection (from the D_2 to the D_1 state) following vertical excitation. A full analysis of the accessibility of the crossing would require CASPT2 re-optimization of the D_1/D_2 crossing geometry. However, at the present time, there are no available, implemented procedures for optimization of conical intersection geometries using CASPT2 gradients.

Basis set effects were analyzed for the CASSCF and multireference calculations. Three basis sets were compared. The 6-31G* basis set was compared with two correlation consistent basis sets (cc-pVTZ and aug-cc-pVTZ) designed to recover correlation energies for multi-reference calculations. The results for CASSCF and CASPT2 at the D_2 minimum and the D_1/D_2 CI are summarized in Table 4. As expected, basis set effects are much more pronounced for the CASPT2 calculation than for the CASSCF. Increasing the basis set for CASSCF does not significantly change the relative energies of the two states and the position of the crossing remains constant. For the CASPT2 calculations, increasing the size of the basis set progressively decreases the energy gap between the D_1 and D_2 states at the D_2 minimum from 20 to 17 kcal/mol and increases the gap at the D_1/D_2 crossing from 6 to 7 kcal/mol (Table 4). As expected, these results indicate that a larger proportion of the correlation energy is recovered with a larger basis set with more polarized functions. From this we can predict that the D_1/D_2 crossing geometry will relax even further with larger basis sets and more highly correlated treatments, meaning that the energy of the crossing may be reduced even further than suggested by Figure 6.

The relative energy changes of the D_1 and D_0 surfaces will also affect the D_0/D_1 crossing. Comparing the CASSCF and CASPT2 energies with a cc-pVTZ basis (Table 3), we see that the energy gap between D_0 and D_1 at the D_1 minimum has

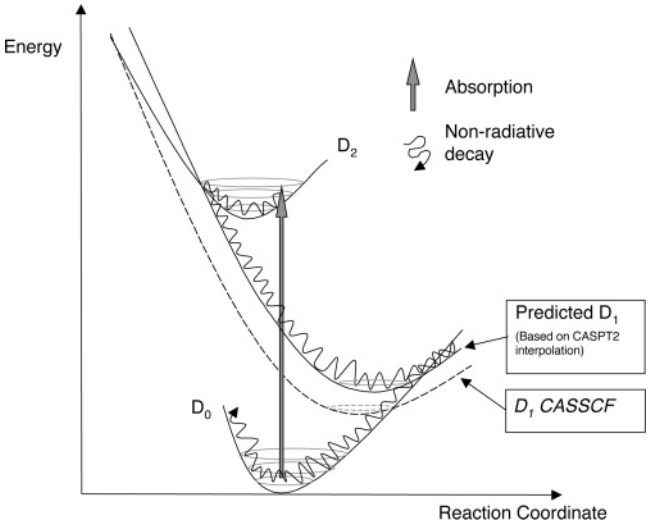

Figure 7. Schematic representation of the electronic relaxation mechanism of the naphthalene radical cation. Dashed curve: original CASSCF/6-31G* result for D_1 state. Solid curve: predicted relative increase in D_1 energies indicated by CASPT2 calculations that suggests a lower energy D_1/D_2 CI, allowing for nonradiative relaxation.

increased by 8 kcal/mol with CASPT2. However, the position of the crossing has also changed, because the D_1 state is 8 kcal/mol higher than the D_0 state at the CASSCF optimized D_0/D_1 CI when the energy is re-computed with CASPT2. Thus, the barrier to the crossing from the D_1 minimum is not expected to change significantly. Also, the barrier to the crossing from the D_1 minimum calculated with CASSCF is so small (1.6 kcal/mol) that small changes in the barrier height would not substantially affect the accessibility of the crossing following vertical excitation.

Figure 7 shows a schematic representation of the form of the PESs for the naphthalene cation system, showing the CASSCF result for the D_1 state (dashed curve) together with the required relative increase in the energy of D_1 suggested by the CASPT2 results (solid curve). With sufficient relaxation of the energy of the D_1/D_2 CI, our results support a mechanism for the ultrafast relaxation of the photoexcited naphthalene radical cation in agreement with experimental observation.

The Zhao group proposed a $D_2 \rightarrow D_1$ relaxation occurring within approximately 1 fs. Initial CASSCF results do not support this. However, subsequent CASPT2 calculations indicate that $\sigma-\pi$ dynamic correlation effects, which are not accounted for in the CASSCF treatment, are important in the relative positions of the energy surfaces. This causes an effective lowering of the energy of the D_0 and D_2 states relative to the D_1 state. The result is a relaxation of the geometry of the D_1/D_2 crossing, bringing it lower in energy and reducing the barrier to the CI from the D_2 minimum. The geometry of the D_1/D_2 crossing is likely to relax further with a more highly correlated treatment, and so the energy of the crossing may be further reduced with a larger basis set. Furthermore, the energy gap between the D_1 and D_2 states reduces rapidly close to the crossing due to the near-parallel gradients of the states as they approach each other. This may mean that nonradiative decay can occur across the small energy gap long before the crossing is reached.

Conclusions

The optimized D_0/D_1 crossing is readily accessible at the CASSCF level, and the energy barrier to the crossing from the D_1 minimum does not appear to change significantly upon inclusion of dynamic correlation energy. However, the relative energy and geometry of the D_1/D_2 crossing do appear to be significantly affected by dynamic correlation. Linear interpolation using CASPT2 indicates that the energy of the D_1/D_2 crossing is significantly lower than with CASSCF, reducing the barrier to the crossing from the D_2 minimum by almost 50% compared with the original CASSCF value. Although these results cannot accurately reproduce energetics consistent with experimental relaxation times ($<$200 fs), they do indicate that an improved treatment of dynamic correlation will further lower the energy barrier to the D_1/D_2 conical intersection, such that it becomes energetically accessible following photoexcitation to the second excited state.

Our results, therefore, support an ultrafast, unimolecular, radiationless decay mechanism between the optically active second excited state and the ground state of the naphthalene radical cation via internal conversion through two consecutive sloped conical intersections. This would explain the observed lack of fluorescence from D_1 or D_2. However, it is not clear from our results why relaxation from the D_2 state to the D_1 state should be even faster than the 200 fs time period calculated for the D_1 to D_0 internal conversion, as was suggested by the experimental results.[12]

The sloped nature of the two optimized crossings indicates that there is a single well-defined energy-lowering coordinate from each intersection, leading only to regeneration of ground state reactants, and explaining the observed photostability of the naphthalene radical cation.

Acknowledgment. This work has been partly supported by EPSRC UK (Grant GR/S94704/01). MOLPRO calculations were performed using computational resources made available via the EPSRC-funded National Service for Computational Chemistry Software (www.nsccs.ac.uk). We thank Paul Donaldson for discussions concerning transient grating spectroscopy, and Dr. Lluís Blancafort for implementing the TDM code in a development version of Gaussian.

References and Notes

(1) Jochims, H. W.; Baumgartel, H.; Leach, S. *Astrophys. J.* **1999**, *512*, 500−510.

(2) Hirama, M.; Tokosumi, T.; Ishida, T.; Aihara, J. *Chem. Phys.* **2004**, *305*, 307−316.

(3) Pope, C. J.; Marr, J. A.; Howard, J. B. *J. Phys. Chem.* **1993**, *97*, 11001−11013.

(4) (a) Berlin, Y. A.; Hutchison, G. R.; Rempala, P.; Ratner, M. A.; Michl, J. *J. Phys. Chem. A* **2003**, *107*, 3970−3980. (b) Grozema, F. C.; Siebbeles, L. D. A.; Gelinck, G. H.; Warman, J. M. The opto-electronic properties of isolated phenylenevinylene molecular wires. In *Molecular Wires: From Design to Properties*; DeCola, L., Ed.; Springer-Verlag Berlin: Berlin, 2005.

(5) Klauk, H.; Gundlach, D. J.; Jackson, T. N. *IEEE Electron Device Lett.* **1999**, *20*, 289−291.

(6) (a) Oomens, J.; Tielens, A.; Sartakov, B. G.; von Helden, G.; Meijer, G., *Astrophys. J.* **2003**, *591*, 968−985. (b) Gotkis, Y.; Oleinikova, M.; Naor, M.; Lifshitz, C. *J. Phys. Chem.* **1993**, *97*, 12282−12290. (c) Ling, Y.; Lifshitz, C. *J. Mass Spectrom.* **1997**, *32*, 1219−1225. (d) Ho, Y. P.; Yang, Y. C.; Klippenstein, S. J.; Dunbar, R. C. *J. Phys. Chem.* **1995**, *99*, 12115−12124.

(7) Heger, M. L. *Lick Obs. Bull.* **1922**, 146.

(8) (a) Salama, F.; Galazutdinov, G. A.; Krelowski, J.; Allamandola, L. J.; Musaev, F. A. *Astrophys. J.* **1999**, *526*, 265−273. (b) Jenniskens, P.; Desert, F. X. *Astron. Astrophys., Suppl. Ser.* **1994**, *106*, 39−78. (c) Snow, T. P. *Spectrochim Acta A* **2001**, *57*, 615−626.

(9) (a) Salama, F.; Allamandola, L. J. *Astrophys. J.* **1992**, *395*, 301−306. (b) Salama, F.; Allamandola, L. J. *J. Chem. Phys.* **1991**, *94*, 6964−6977.(c) Salama, F.; Joblin, C.; Allamandola, L. J. *J. Chem. Phys.* **1994**, *101*, 10252−10262. (d) Ruiterkamp, R.; Halasinski, T.; Salama, F.; Foing, B. H.; Allamandola, L. J.; Schmidt, W.; Ehrenfreund, P. *Astron. Astrophys.* **2002**, *390*, 1153−1170.

(10) (a) Biennier, L.; Salama, F.; Allamandola, L. J.; Scherer, J. J. *J. Chem. Phys.* **2003**, *118*, 7863−7872. (b) Romanini, D.; Biennier, L.; Salama, F.; Kachanov, A.; Allamandola, L. J.; Stoeckel, F. *Chem. Phys. Lett.* **1999**, *303*, 165−170.

(11) (a) Du, P.; Salama, F.; Loew, G. H. *Chem. Phys.* **1993**, *173*, 421−437. (b) Andruniow, T.; Pawlikowski, M. *Chem. Phys.* **1998**, *236*, 25−33. (c) Bally, T.; Carra, C.; Fulscher, M. P.; Zhu, Z. D. *J. Chem. Soc., Perkin Trans.* **1998**, *2*, 1759−1765. (d) da Silva, D. A.; Friedlein, R.; Coropceanu, V.; Ohrwall, G.; Osikowicz, W.; Suess, C.; Sorensen, S. L.; Svensson, S.; Salaneck, W. R.; Bredas, J. L. *Chem. Commun.* **2004**, 1702−1703. (e) Weisman, J. L.; Mattioda, A.; Lee, T. J.; Hudgins, D. M.; Allamandola, L. J.; Bauschlicher, C. W.; Head-Gordon, M. *Phys. Chem. Chem. Phys.* **2005**, *7*, 109−118.

(12) Zhao, L.; Lian, R.; Shkrob, I. A.; Crowell, R. A.; Pommeret, S.; Chronister, E. L.; Liu, A. D.; Trifunac, A. D. *J. Phys. Chem. A* **2004**, *108*, 25−31.

(13) (a) Klessinger, M.; Michl, J. *Excited States and Photochemistry of Organic Molecules*; VCH: New York, 1995; pp 182−186. (b) Blancafort, L.; Ogliaro, F.; Olivucci, M.; Robb, M. A.; Bearpark, M. J.; Sinicropi, A., Computational Investigation of Photochemical Reaction Mechanisms. In *Computational Methods in Photochemistry*; Kutateladze, A. G., Ed.; CRC Press: Boca Raton, FL, 2005. (c) Robb, M. A.; Garavelli, M.; Olivucci, M.; Bernardi, F., A computational strategy for organic photochemistry. In *Reviews in Computational Chemistry*; Lipkowitz, K. B., Boyd, D. B., Eds.; Wiley-VCH, Inc.: New York, 2000. (d) Bernardi, F.; Olivucci, M.; Robb, M. A. *Chem. Soc. Rev.* **1996**, *25*, 321−328. (e) Yarkony, D. R. *Rev. Mod. Phys.* **1996**, *68*, 985−1013.

(14) (a) Paterson, M. J.; Robb, M. A.; Blancafort, L.; DeBellis, A. D. *J. Am. Chem. Soc.* **2004**, *126*, 2912−2922. (b) Ben-Nun, M.; Molnar, F.; Schulten, K.; Martinez, T. J. *Proc. Natl. Acad. Sci. U.S.A.* **2002**, *99*, 1769−1773. (c) Yarkony, D. R. *J. Chem. Phys.* **2001**, *114*, 2601−2613.

(15) Atchity, G. J.; Xantheas, S. S.; Ruedenberg, K. *J. Chem. Phys.* **1991**, *95*, 1862−1876.

(16) Boggio-Pasqua, M.; Robb, M. A.; Bearpark, M. J., *J. Phys. Chem. A* **2005**, *109*, 8849−8856.

(17) Bearpark, M. J.; Bernardi, F.; Clifford, S.; Olivucci, M.; Robb, M. A.; Smith, B. R.; Vreven, T. *J. Am. Chem. Soc.* **1996**, *118*, 169−175.

(18) (a) Raghavachari, K.; Haddon, R. C.; Miller, T. A.; Bondybey, V. E. *J. Chem. Phys.* **1983**, *79*, 1387−1395. (b) Applegate, B. E.; Miller, T. A., *J. Chem. Phys.* **2002**, *117*, 10654−10674. (c) Vysotsky, V. P.; Salnikov, G. E.; Shchegoleva, L. N. *Int. J. Quantum Chem.* **2004**, *100*, 469−476.

(19) Blancafort, L.; Jolibois, F.; Olivucci, M.; Robb, M. A. *J. Am. Chem. Soc.* **2001**, *123*, 722−732.

(20) Frisch, M. J.; Trucks, G. W.; Schlegel, H. B.; Scuseria, G. E.; Robb, M. A.; Cheeseman, J. R.; Montgomery, J., J. A.; Vreven, T.; Kudin, K. N.; Burant, J. C.; Millam, J. M.; Iyengar, S. S.; Tomasi, J.; Barone, V.; Mennucci, B.; Cossi, M.; Scalmani, G.; Rega, N.; Petersson, G. A.; Nakatsuji, H.; Hada, M.; Ehara, M.; Toyota, K.; Fukuda, R.; Hasegawa, J.; Ishida, M.; Nakajima, T.; Honda, Y.; Kitao, O.; Nakai, H.; Klene, M.; Li, X.; Knox, J. E.; Hratchian, H. P.; Cross, J. B.; Bakken, V.; Adamo, C.; Jaramillo, J.; Gomperts, R.; Stratmann, R. E.; Yazyev, O.; Austin, A. J.; Cammi, R.; Pomelli, C.; Ochterski, J. W.; Ayala, P. Y.; Morokuma, K.; Voth, G. A.; Salvador, P.; Dannenberg, J. J.; Zakrzewski, V. G.; Dapprich, S.; Daniels, A. D.; Strain, M. C.; Farkas, O.; Malick, D. K.; Rabuck, A. D.; Raghavachari, K.; Foresman, J. B.; Ortiz, J. V.; Cui, Q.; Baboul, A. G.; Clifford, S.; Cioslowski, J.; Stefanov, B. B.; Liu, G.; Liashenko, A.; Piskorz, P.; Komaromi, I.; Martin, R. L.; Fox, D. J.; Keith, T.; Al-Laham, M. A.; Peng, C. Y.; Nanayakkara, A.; Challacombe, M.; Gill, P. M. W.; Johnson, B.; Chen, W.; Wong, M. W.; Gonzalez, C.; Pople, J. A. *Gaussian Development Version, Revision B.07*, Gaussian, Inc.: Wallingford, CT, 2003.

(21) Werner, H.-J.; Knowles, P. J.; Lindh, R.; Manby, F. R.; Schutz, M.; Celani, P.; Korona, T.; Rauhut, G.; Amos, R. D.; Bernhardsson, A.; Berning, A.; Cooper, D. L.; Deegan, M. J. O.; Dobbyn, A. J.; Eckert, F.; Hampel, C.; Hetzer, G.; Lloyd, A. W.; McNicholas, S. J.; Meyer, W.; Mura, M. E.; Nicklass, A.; Palmieri, P.; Pitzer, R.; Schumann, U.; Stoll, H.; Stone, A. J.; Tarroni, R.; Thorsteinsson, T. *MOLPRO*, 2002.6; Birmingham, UK, 2003.

(22) Hehre, W. J.; Ditchfield, R.; Pople, J. A. *J. Chem. Phys.* **1972**, *56*, 2257. Harihara, P. C.; Pople, J. A., *Theor. Chim. Acta* **1973**, *28*, 213−222.

(23) Dunning, T. H., *J. Chem. Phys.* **1989**, *90*, 1007−1023.

(24) Kendall, R. A.; Dunning, T. H.; Harrison, R. J. *J. Chem. Phys.* **1992**, *96*, 6796−6806.

(25) Hehre, W. J.; Stewart, R. F.; Pople, J. A. *J. Chem. Phys.* **1969**, 2657.

(26) Knowles, P. J.; Werner, H. J. *Chem. Phys. Lett.* **1988**, *145*, 514−522. Werner, H. J.; Knowles, P. J. *J. Chem. Phys.* **1988**, *89*, 5803−5814.

(27) Celani, P.; Werner, H. J. *J. Chem. Phys.* **2000**, *112*, 5546−5557.

(28) Bearpark, M. J.; Robb, M. A.; Schlegel, H. B. *Chem. Phys. Lett.* **1994**, *223*, 269−274.

(29) Brock, C. P.; Dunitz, J. D. *Acta Crystallogr., Sect. B* **1982**, *38*, 2218−2228.

(30) Boggio-Pasqua, M.; Bearpark, M. J.; Ogliaro, F.; Robb, M. A. *J. Am. Chem. Soc.* **2006**, *128*, 10533−10540.

(31) Eland, J. H. D; Danby, C. J. *Z. Naturforsch., A: Phys. Sci.* **1968**, *23*, 355.